Materials Science & Engineering A 860 (2022) 144294

Contents lists available at ScienceDirect

Materials Science & Engineering A

journal homepage: www.elsevier.com/locate/msea

Determination of α to β phase transformation kinetics in laser-powder bed fused Ti–6Al–2Sn–4Zr–2Mo-0.08Si and Ti–6Al–4V alloys

Harish Chandra Kaushik [a], Mahdi Habibnejad Korayem [b], Amir Hadadzadeh [a,*]

[a] Department of Mechanical Engineering, University of Memphis, Memphis, TN, USA
[b] AP&C Advanced Powder and Coating, a GE Additive Company, Montreal, Quebec, Canada

ARTICLE INFO

Keywords:
Additive manufacturing
Phase transformation kinetics
Differential scanning calorimetry
JMAK model
Titanium alloys

ABSTRACT

Laser powder bed fused (L-PBF) Ti–6Al–2Sn–4Zr–2Mo-0.08Si (L-PBF-Ti-6242) and two grades of L-PBF-Ti-6Al–4V (L-PBF-Ti-64) alloys are studied using differential scanning calorimetry (DSC), to determine the kinetics of α to β phase transformation to design and develop post-process heat treatments. Both non-isothermal and isothermal kinetics models are developed using the DSC results and employing the Johnson-Mehl-Avrami-Kolmogorov (JMAK) equation. The mechanism of non-isothermal phase transformation is discussed based on the local Avrami parameters. The transformation process is divided into three stages showing a high rate of transformation in the initial stage (dominated by nucleation) followed by a steady-state rate (dominated by growth) and again a rapid increase in the transformation rate in the final stage. The effect of the β stabilizing elements on α to β phase transformation kinetics is discussed for all three alloys in both non-isothermal and isothermal transformations. L-PBF-Ti-6242 needs higher activation energy to initiate the transformation and the process occurs at a comparatively higher temperature range since this is a near-α Ti alloy. The oxygen homogeneity in the L-PBF-Ti-64 shows a clear effect on the transformation kinetics. The initial microstructure also affects the kinetics of α to β phase transformation, as the as-built L-PBF microstructure results in the highest transformation kinetics. Any heat treatment that alters the as-built microstructure results in slower transformation kinetics. The results of the isothermal kinetics models are employed to design a two-step heat treatment for L-PBF-Ti-6242 to enhance the ductility with minimal strength loss. The properties are then correlated to the microstructure. This study provides great insight into the importance of considering the effect of the material system, alloying elements, and initial microstructure on the kinetics of phase transformation in L-PBF titanium alloys and the role of phase transformation kinetics in designing heat treatments to achieve the desired microstructure and properties.

1. Introduction

Titanium and its alloys possess excellent ambient and high-temperature corrosion resistance and strength, which makes them an attractive material for advanced applications. Pure titanium with moderate strength can meet the corrosion resistance requirements for some applications such as heat exchangers, chemical processing reactors, and petrochemical vessels. On the other hand, titanium alloys have been developed based on the microstructure-property relationship, considering the application. For instance, Ti–6Al–4V (Ti-64), an α+β titanium alloy, has been developed to achieve higher strength at room and elevated temperatures for applications like medical implants, and automotive components with moderate service temperatures. Further developments have been achieved for higher temperature applications; for instance, Ti–6Al–2Sn–4Zr–2Mo-0.08Si (Ti-6242), a near alpha (α) alloy, has high-temperature applications like aero-engine components, supersonic military aircraft, and gas turbines [1,2]. Ti-64 is the most common titanium alloy in the aerospace industry. It has aluminum and vanadium elements as α and β stabilizers, respectively. The presence of both α and β phases at room temperature gives excellent yield strength and ductility to Ti-64 [3]. The 4–6% of beta stabilizer makes it a heat-treatable alloy. The β phase transformed to martensite (α') during solidification when vanadium concentration is less than 4.27 at% in the β phase [4]. Nevertheless, high-temperature applications are limited to temperatures up to 400°C [5]. On the other hand, Ti-6242 is used for long-term high-temperature applications up to 540°C with better creep

* Corresponding author.
E-mail address: amir.hadadzadeh@memphis.edu (A. Hadadzadeh).

https://doi.org/10.1016/j.msea.2022.144294
Received 29 August 2022; Received in revised form 18 October 2022; Accepted 3 November 2022
Available online 8 November 2022

and fatigue properties [6–8]. Ti-6242 has aluminum as α and molybdenum as β-stabilizer elements. Aluminum works as a solution-strengthening element whereas tin and zirconium play the same role with minimal influence in stabilizing a particular phase. Adding a limited percentage of silicon, up to 0.25 wt%, improves high-temperature creep resistance [9,10].

The allotopic α to β phase transformation in titanium plays an important role in the physical and mechanical properties of this material. This solid-state phase transformation is a key parameter in determining the heat treatment process to achieve the desired microstructure. Since the alloying elements may stabilize a phase (α or β), the α to β transus temperature varies in different titanium alloys. Moreover, the starting microstructure for a given alloy can alter the transus temperature. Therefore, a systematic and scientific study is required to determine the kinetics of phase transformation in titanium alloys. Differential scanning calorimetry (DSC) is a powerful tool to achieve such a goal. Homporova et al. [11] studied the β to α phase transformation in an annealed Ti-64 alloy in α+β and β regions with different cooling rates. The purpose of the study was to determine the conditions that result in various microstructures in terms of the size and morphology of α-laths and primary α-grains in β matrix, α', and secondary α. Xu et al. [12] investigated the α' phase transformations by performing DSC on Ti-64 samples. The samples were heat treated at 850 °C, 900 °C, and 950 °C. The authors observed broader and deeper exothermic peaks for samples heat treated at higher temperatures due to higher α' proportion in the matrix and reported that α' nucleation rate is proportional to the vanadium content in the β phase. Steedman et al. [13] performed DSC runs to analyze aluminum and vanadium in-situ diffusion under varying holding times at 1200 °C for a powder blend of fine and coarse 60Al–40V and CP-Ti (Grade 3). The DSC results disclosed a more flat and broad transformation peak and high β transus temperature for a short holding time and revealed faster diffusion of Al than V. An opposite trend was seen for a longer holding time where V diffuses much faster. Hardy et al. [14] performed a DSC test on an aged Ti-64 sample to analyze α' to α+β phase transformation for continuous heating and the results also revealed the secondary α dissolution temperature. Li et al. [15] used DSC to pick the correct heat treatment temperature to achieve high strength in porous Ti-64 components for medical applications.

The literature has a limited body of work on the analysis of phase transformation in Ti-6242. Reiger et al. [16] studied Ti-6242 to identify the β transus temperature and verified the result by quantitative analysis of phase content. The result shows an increase in β content from 62 vol% to 96 vol% for temperature increase from 980 °C to 1015 °C and 100 vol % at 1020 °C. The authors also performed EDX-SEM analysis and showed a high percentage of β and α stabilizing elements in α' and α phases, respectively. To our best knowledge, no literature is available on the modeling of phase transformation kinetics in L-PBF-Ti-6242. The study of phase transformation kinetics is important to establish fundamental knowledge of the role of material history in physical properties. The material history in terms of chemistry (α and β stabilizer elements) and processing (manufacturing route and heat treatment) will affect the microstructure which will then determine the physical properties. As a result, the kinetics of phase transformation will alter. One important aspect of the phase transformation kinetics should be sought in optimizing the heat treatment parameters to obtain desired microstructure and properties. Literature reports some studies to establish the empirical relationship between heat treatment and the microstructure of titanium alloys [17,18], but modeling of phase transformation kinetics is still limited. Malinov et al. [19] used DSC data of continuous cooling of Ti-64 to model β to α phase transformation kinetics by employing Johnson-Mehl-Avrami-Kolmogorov (JMAK) model. The study showed that the transformation is controlled by the nucleation rate and the activation energy for nucleation is inversely proportional to temperature. Yu et al. [20] employed thermal dilatometry to investigate the non-isothermal phase transformation of Ti-64 and used JMAK theory to model the kinetics. The obtained transformation curve shows typical "S" patterns designating the elemental diffusion-controlled nucleation and growth mechanism.

It is noteworthy to mention that the rate of phase transformation does not only depend on the composition of the alloy and the heating rate, but it also depends upon the initial microstructure. Fan. et al. [21] discussed the effect of initial microstructure in the transformation kinetics of TA15 titanium alloy, another near α alloy, and showed that the rate of phase transformation is different for different initial microstructures as it changes from equiaxed α to lamellar α. In another study, Li et al. [22] discussed the phase transformation kinetics of equiaxed, duplex, and lamellar structures as the initial microstructure of Ti-64-0.55Fe. The work reported that the lamellar structure has the highest activation energy and the fastest rate of α to β transformation while equiaxed has the lowest activation energy with the slowest transformation rate.

Titanium alloys have been fabricated through conventional manufacturing processes including casting, rolling, forging, etc. However, an obstacle to the widespread application of titanium alloys is the high cost of production, mainly raised from the machining step [23]. Therefore, an alternative way to reduce production costs is to adopt a near-net-shape manufacturing route. Among the available near-net-shape manufacturing processes, powder metallurgy (PM) and additive manufacturing (AM) techniques have shown potential for the fabrication of titanium alloys [24]. However, AM processes, in specific powder bed fusion (PBF) techniques, possess unique characteristics that make them attractive for the fabrication of titanium components. Laser-PBF (L-PBF) has shown promise in terms of fabricating metallic alloys with enhanced mechanical properties [24]. Therefore, investigation of the L-PBF of titanium alloys is essential to develop knowledge on the processing-microstructure-properties relationship in these alloys to spread their application.

The fabrication of metallic materials using metal AM processes, and in particular L-PBF, results in the evolution of a unique microstructure. The high cooling rate associated with the L-PBF process (in the range of 10^3–10^8 K/s) is the dominant factor in the evolution of ultrafine, metastable, and hierarchical microstructures [25]. There are available studies on the role of such unique microstructures in the mechanical properties of L-PBF alloys [25–29]. While there are studies available on the role of hierarchical microstructures in phase transformations [30], the role of hierarchical microstructures in phase transformation kinetics has not been investigated. Such microstructures can potentially alter the kinetics (and even thermodynamics) of phase transformations in the L-PBF materials. For instance, it has been reported that the dislocation density can substantially affect the precipitation kinetics [31,32] since dislocations act as pipelines for the diffusion of alloying elements. One of the hierarchical characteristics in the microstructure of L-PBF alloys is the high dislocation density [25]. While in some cases such as high entropy alloys the dislocation density may vary depending on the build height location [33], in legacy alloys like AlSi10Mg and Ti-64 the dislocation density is almost consistent at different heights [34,35]. Considering the high dislocation density in the L-PBF alloys, the kinetics of phase transformation could be potentially different compared to the conventionally manufactured counterparts. Therefore, it is necessary to develop a fundamental understanding of the role of metastable and hierarchical microstructure in the α to β phase transformation kinetics in L-PBF-titanium alloys.

The development of α to β phase transformation kinetics in L-PBF-titanium alloys will create a basis for the development of proper heat treatment recipes to design desired microstructures and properties. The available studies on the heat treatment of L-PBF-Ti-64 [36,37] and L-PBF-Ti-6242 [16,38,39] show that different heat treatment recipes have been employed by different researchers that have resulted in a variety of microstructures. However, it appears these heat treatments were developed based on trial and error efforts rather than knowing the kinetics of phase transformations. This study can shed the light on a scientific and optimum approach to designing the proper heat

treatments for L-PBF-titanium alloys.

In the present work, the kinetics of α to β transformation of L-PBF-Ti-6242 and two grades of L-PBF-Ti-64 alloys are modeled using the DSC results. The difference between the two Ti-64 grades is the homogeneity of oxygen distribution in their chemistry. The DSC runs are performed under non-isothermal heating and the modeled parameters are employed to develop the isothermal heating conditions. The modified Johnson-Mehl-Avrami-Kolmogorov (JMAK) model is used for the modeling of phase transformation kinetics. Literature shows the importance and efficiency of the JMAK model to investigate the phase transformation kinetics of metallic alloys like Ti-64 [19,20], steel [40], and amorphous alloys [41,42].

2. Experimental procedure

2.1. Materials and L-PBF process

L-PBF technique was used to fabricate cylindrical rods of Ti-6242 and Ti-64 in a vertical orientation with 8 mm diameter and 70 mm height using the EOS M290 machine available at the University of Memphis (Metal Additive Manufacturing Laboratory). The L-PBF process parameters to fabricate all the alloys remained the same to attain comparable results. Important process parameters include laser power (P), scan speed (v), hatch distance (l), and layer thickness (h). In the current study, these parameters were selected based on the optimum parameters developed for the fabrication of the titanium alloys with the least porosity level and set to $P = 280$ W, $v = 1200$ mm/s, $l = 140$ μm, and $h = 30$ μm. The samples were printed using the stripe scanning strategy. Two grades of Ti-64 powder were used to fabricate the rods, namely grade 23 (Ti-64-G23 which is equivalent to Ti-64 ELI) and a mixed grade (Ti-64-MG). The difference between these grades is their oxygen homogeneity. While in both grades the oxygen content is less than the 0.2 wt% standard thresholds, the distribution of the oxygen element is different. In Ti-64-G23, the oxygen is distributed homogeneously in all interstitial positions in the crystal structure. On the other hand, the Ti-64-MG powder was produced by mixing a low-oxygen-content powder (Ti-64-G23) and a high-oxygen-content powder (Ti-64-G5). It is well-known that the oxygen content in titanium alloys should be carefully monitored due to its role in the microstructure evolution [43–45]. While the overall oxygen content was kept at 0.13 wt%, the positions with a higher percentage of Ti-64-G5 contribute higher oxygen content compared to positions with higher Ti-64-G23 particles. The main motivation in this regard was to investigate the feasibility of grade mixtures for various processes of additive manufacturing in which the oxygen content needs to be controlled. The chemical composition of the powders is shown in Table 1 and Table 2. The powder feedstocks were supplied by AP&C (a GE Additive Company) in Quebec, Canada with a particle size distribution of 15–45 μm.

2.2. DSC analysis

To study the thermal behavior of the alloys, DSC tests were performed using an SDT 650, TA instruments (Delaware, USA). The continuous flow of highly pure argon gas with a flow rate of 150 mL/min was maintained to eliminate oxidation. To perform DSC analysis, small discs of 4 mm diameter and 2 mm height were machined from the L-PBF samples with a flat base to achieve uniform heat flow. The samples were made from the centerline of the rods, away from the top and bottom of the component to ensure the consistency and repeatability of the results. To study the non-isothermal phase transformation kinetics, continuous heating was conducted at a heating rate (Φ) of 20, 30, 40, and 50 °C/min from room temperature to 1200 °C. All the calculations to model the transformation kinetics were done on the baseline-corrected curves. The baseline correction was done using the peak analyzer module of OriginPro 2021. To study the effect of initial microstructure on transformation kinetics ten repeated heating and cooling runs were done on the L-PBF-Ti-6242 at a heating rate of 20 °C/min from room temperature to 1200 °C. It is noteworthy to mention that despite the nature of the L-PBF technique in accumulating heat during layer-by-layer deposition, the microstructure of L-PBF alloys is relatively consistent through the height of a cylindrical rod from bottom to top [35]. Therefore, the DSC results in the current study represent the behavior of the L-PBF material at different build heights.

Table 1
Chemical composition of Ti-6242 feedstock (wt%).

Alloy	Al	Sn	Zr	Mo	Si	Ti
Ti-6242	6	2	4	2	0.08	Bal.

2.3. Microstructural studies

The microstructure of L-PBF-Ti-6242 was studied using the scanning electron microscopy (SEM) technique. The samples were prepared through a standard metallography procedure followed by etching using Kroll's Reagent. The SEM imaging was done using a field emission gun scanning electron microscope (FEG-SEM-FEI Nova NanoSEM-650). All images were taken in the secondary electron (SE) mode.

3. Results and discussion

3.1. Evaluation of DSC results and baseline correction

Titanium has a hexagonal close-packed crystal structure at room temperature and a body-centered cubic structure at higher temperatures known as α and β phases, respectively. Fig. 1 (a) shows the DSC curves for L-PBF-Ti-6242 from 200 °C to 1200 °C for varying heating rates of 20, 30, 40, and 50 °C/min. The DSC curves represent some exothermic and endothermic reactions in the material associated with the phase transformations. Fig. 1 (a) shows the DSC curves of L-PBF-Ti-6242 for varying heating rates. Two important peaks are highlighted on the curve; nanotwin annihilation (an exothermic peak) and α to β transformation (an endothermic peak) zones; labeled as peak 1 and peak 2, respectively. Nanotwins are formed during the L-PBF process due to rapid cooling [46]. Previous studies have shown the importance of nanotwins in enhancing the material's ductility by accommodating the dislocations [47]. Therefore, in the process of designing the heat treatment of the L-PBF-Ti-6242, it is important to consider this zone to preserve the nanotwins. On the other hand, the study of α to β transformation zone (peak 2) is important to determine the β-transus temperature which plays a crucial role to optimize the solutionizing temperature. The β-transus temperature is the temperature for the transformation of all α to β [48].

The reaction considered in the current study is the endothermic process that is associated with the α to β transformation. To better study these endothermic peaks and determine their characteristics, the DSC curves were corrected by subtracting the baseline. The baseline subtraction eliminates the artifacts and nonlinearities that emerge from the DSC equipment [49] and accounts for the heat flow only due to reaction in the measuring system or sample [50]. Each peak is characterized by three temperatures: onset (T_o), peak (T_P), and end (T_e) temperatures [42]. The T_o and T_e temperatures represent the start and completion points of the process, while the T_P is associated with the highest phase transformation rate represented by the half-width of the peak (sharpness of the peak). The baseline subtraction is performed between the T_o and T_e for each heating rate. The T_o and T_e is determined using the first derivative of heat flow as a function of temperature as shown in Fig. 1 (b). The peak in derivative gives the start and finish of a transformation process as it represents the slope of the actual heat flow curve and highlights the T_o and T_e. Further study is focused in the region between T_o and T_e as shown in Fig. 1 (c), (d) and (e) which represent α to β transformation region after baseline correction for L-PBF-Ti-6242,

Table 2
Chemical composition of Ti-64-MG and Ti-64-G23 feedstock (wt%).

Alloy	Al	V	Fe	O	C	N	H	Y	Other each	Other total	Ti
Ti-64 MG	6.36	4.04	0.21	0.13	0.01	0.01	0.002	<0.001	<0.1	<0.4	Bal.
Ti-64 G23	6.32	3.99	0.19	0.12	0.02	0.01	0.002	<0.001	<0.1	<0.4	Bal.

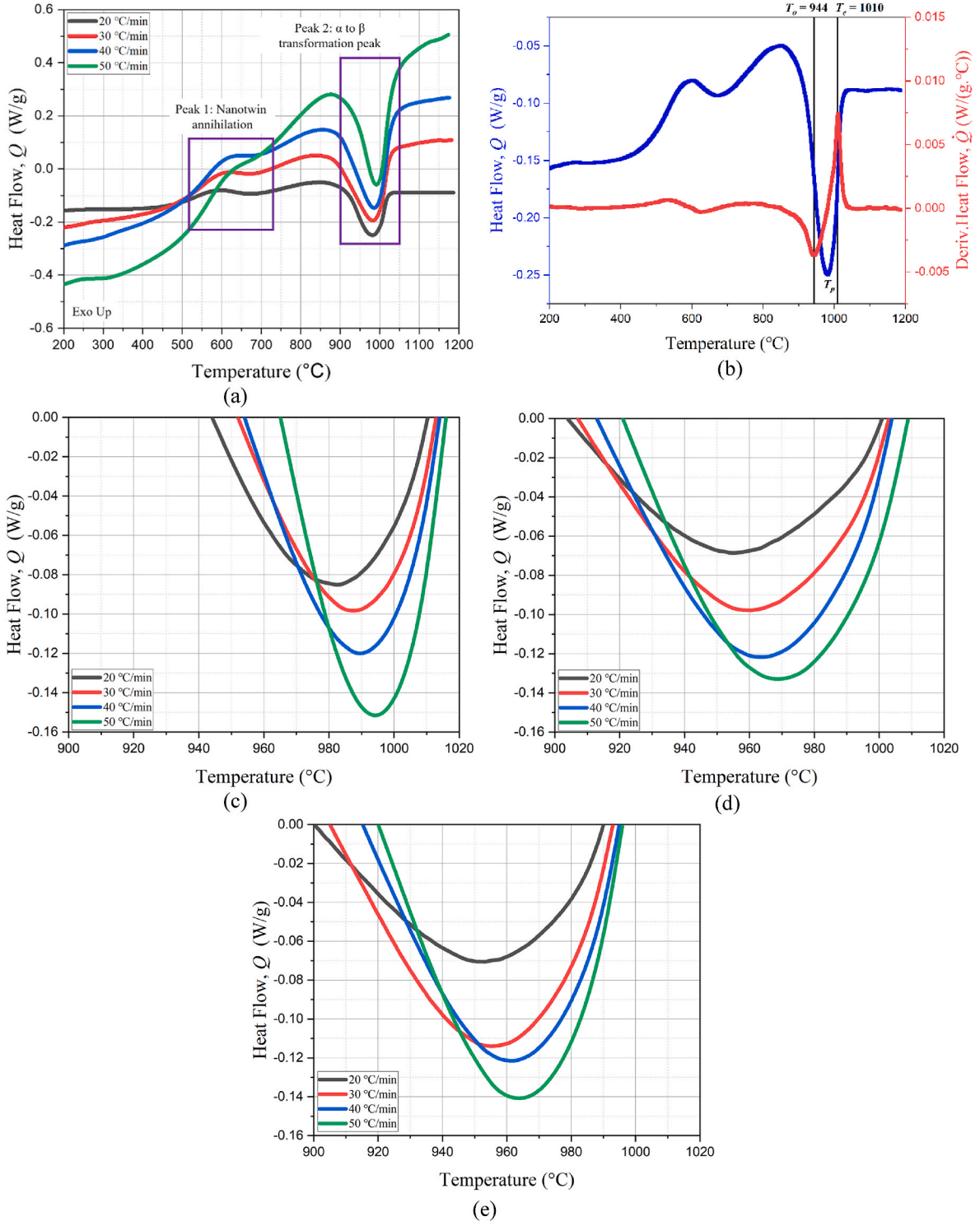

Fig. 1. DSC curves for (a) L-PBF-Ti-6242 without baseline correction and (b) determination of T_o and T_e using first derivative as a function of temperature (for L-PBF-Ti-6242 at a heating rate of 20°C/min). α to β transformation peaks after baseline correction for (c) L-PBF-Ti-6242, (d) L-PBF-Ti-64-MG, and (e) L-PBF-Ti-64-G23.

L-PBF-Ti-64-MG, and L-PBF-Ti64-G23 respectively at various heating rates.

It is noteworthy to mention that a metastable sub-nanometer transition phase forms during the α to β phase transformation in titanium alloys. Fu et al. [51] used in-situ TEM and STEM characterization techniques to analyze the non-classical intermediate states of α to β phase transformation in Ti–Mo binary alloy. The study revealed the formation of a six-fold symmetry hexagonal pattern with lattice parameters different than the original α phase. Wang et al. [30] also reported the formation of a transition phase designated as α_{HME} (high in Mo_{eq}), a non-equilibrium HCP phase having composition close to β phase in the L-PBF-Ti-64 during α' to α+β phase transformation. The α_{HME} has lattice parameters different from the original α' martensite. These studies show the presence of an intermediate stage during the phase transformation, however, due to the sub-nanometer scale of the phase, no heat flow evidence was observed in the DSC curves in the current study.

The area under the peak is the total energy required for the transformation. The β transus temperature (T_e), was evaluated from the DSC curves for L-PBF-Ti-6242, L-PBF-Ti-64-MG, and L-PBF-Ti-64-G23 as 1013 ± 2°C, 1004 ± 3°C, and 993 ± 2°C, respectively. The β transus temperature of L-PBF-Ti-6242 is close to the value reported by Rieger et al. [16]. Among the three alloys analyzed in this study, the highest β transus temperature belongs to L-PBF-Ti-6242 as it is a near-α titanium alloy with the least β stabilizing elements. It is clear from Fig. 1 (c)–(e) that the peak temperature shifts towards a higher value for the higher heating rates. Such a phenomenon could be explained using thermodynamics and kinetics concepts as any reaction needs time to complete. By increasing the heating rate, the time period reduces, so the reaction is completed at a higher temperature. This clear shift in peak temperature for a higher heating rate has been previously reported for other materials [52,53]. Table 3 shows the values of peak temperatures along with the range of onset and end temperatures for the three alloys. L-PBF-Ti-64-MG has a higher peak temperature than L-PBF-Ti-64-G23 for the same heating rates. This may be due to the heterogeneous distribution of oxygen in the L-PBF-Ti-64-MG which delays the kinetics. Among all, L-PBF-Ti-6242 has the least β stabilizing elements that result in the highest peak temperature.

3.2. Activation energy calculation

The calculation of activation energy (E_a) is a prerequisite to studying the transformation kinetics of any system where E_a is generally a constant in the case of single-phase transformation [54]. The activation energy is a thermodynamics parameter that represents the minimum level of energy (*i.e.* energy barrier) required to start a process of transformation. Using the DSC results, the activation energy for α to β transformation in titanium alloys can be estimated using the Kissinger model [55]. The Kissinger model is expressed as follows [56]:

$$\ln\left(\frac{\Phi}{T_p^{\,2}}\right) = -\frac{E_a}{RT_p} + constant \tag{1}$$

Table 3
Comparison of peak temperatures and transformation range as a function of heating rate obtained from the DSC curves.

Φ (°C/min)	L-PBF-Ti-6242	L-PBF-Ti-64-MG	L-PBF-Ti-64-G23
	T_P (°C)		
20	982	955	951
30	987	960	955
40	990	964	961
50	994.5	969	965
	α→β transformation range		
20–50	944–1016	904–1008	900–996

where R is the universal gas constant (8.314 J/mol.K), T_P is the peak temperature (in K), Φ is the heating rate (in K/s) and E_a is the activation energy (in J/mol). The activation energy could be evaluated by using a linear regression between $\ln\left(\frac{\Phi}{T_p^{\,2}}\right)$ and $1000/T_p$ as shown in Fig. 2.

It is observed from Fig. 2 that L-PBF-Ti-6242 has the highest activation energy of 973.73 kJ/mol compared to L-PBF-Ti-64-MG and L-PBF-Ti-64-G23 with respective values of 824.61 and 770.18 kJ/mol for α to β transformation. Such a difference is associated with the characteristics of L-PBF-Ti-6242 since it is a near-α titanium alloy. Consequently, due to the stability of the α phase, L-PBF-Ti-6242 requires more energy to activate the transformation. On the other hand, both L-PBF-Ti-64-MG and L-PBF-Ti-64-G23 alloys possess β stabilizing elements, stimulating the transformation to begin at lower energy levels.

The study further continued to investigate the activation energy of a conventionally manufactured Ti-6242 (rolling in this case). DSC runs with different heating rates were conducted and the activation energy was calculated as seen in Fig. 3. The study shows that the rolled Ti-6242 has an activation energy of 1169.61 kJ/mol which is higher than L-PBF-Ti-6242. The reason might be the formation of a higher number of dislocations during rapid cooling in the L-PBF process. The dense and entangled dislocations will facilitate the diffusion of the alloying elements [31] and consequently expedite the α to β phase transformation. As a result, lower activation energy is achieved in the L-PBF-Ti-6242 alloy.

3.3. Calculation of α to β transformed fraction

The heat flow values obtained from the DSC experiments are used to calculate the transformation percentage at any time (t) using Eq. (2) [57]. The basis for the calculation of the transformed fraction is to compare the fraction of heat absorbed or released to the total heat flow needed to finish the transformation. It is also noteworthy to mention that the denominator in Eq. (2) represents the total enthalpy of transformation and the integration should be taken over time rather than the temperature [57].

$$Y = \frac{\int_{t_s}^{t} H dt}{\int_{t_s}^{t_e} H dt} \tag{2}$$

where Y is the fraction transformed, t_s and t_e are the transformation start and end times, respectively, and H is the heat flow measured during the DSC runs. Quantitatively, the numerator represents the area under the baseline-corrected DSC curve between t_s and t (Fig. 1 (b)–(d)), while the denominator is the total area under the peak curve.

Fig. 4 shows the fraction of α transformed to β as a function of time. The plot shows a typical sigmoidal curve, thus, the α to β transformation process is governed by nucleation and growth mechanisms [20]. Although both L-PBF-Ti-64-MG and L-PBF-Ti-64-G23 have the same weight percentage of oxygen, for a given heating rate, the former requires a longer time for the completion of the transformation. Such a difference could be explained by considering the homogeneity of the oxygen distribution in the chemical composition. As mentioned in section 2.1, the Ti-64-MG powder was produced by mixing a low-oxygen-content powder (Ti-64-G23) and a high-oxygen-content powder (Ti-64-G5). Therefore, it is expected that a heterogeneous oxygen distribution presents in Ti-64-MG. As a result, in the positions where higher local oxygen content is available the kinetics is delayed as oxygen is α stabilizer and the β nucleation is comparatively difficult. On the other hand, in the positions where lower local oxygen content is available, the kinetics of phase transformation is considerably similar to the standard Ti-64-G23. So, the addition of Ti-64-G5 to Ti-64-G23 delays the

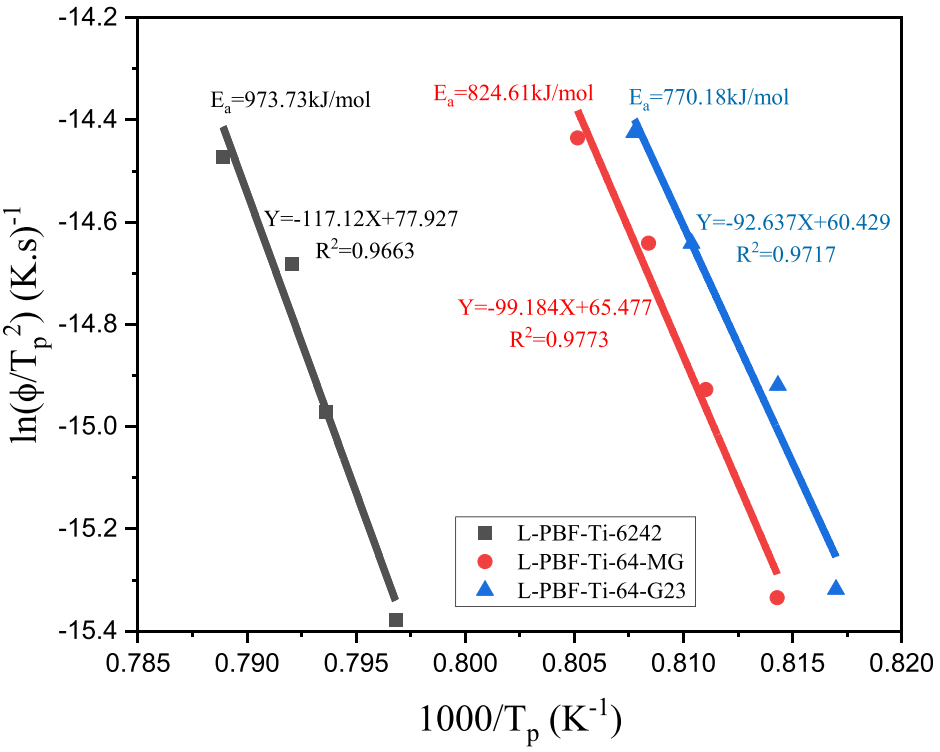

Fig. 2. Kissinger plot for activation energy determination using the DSC results.

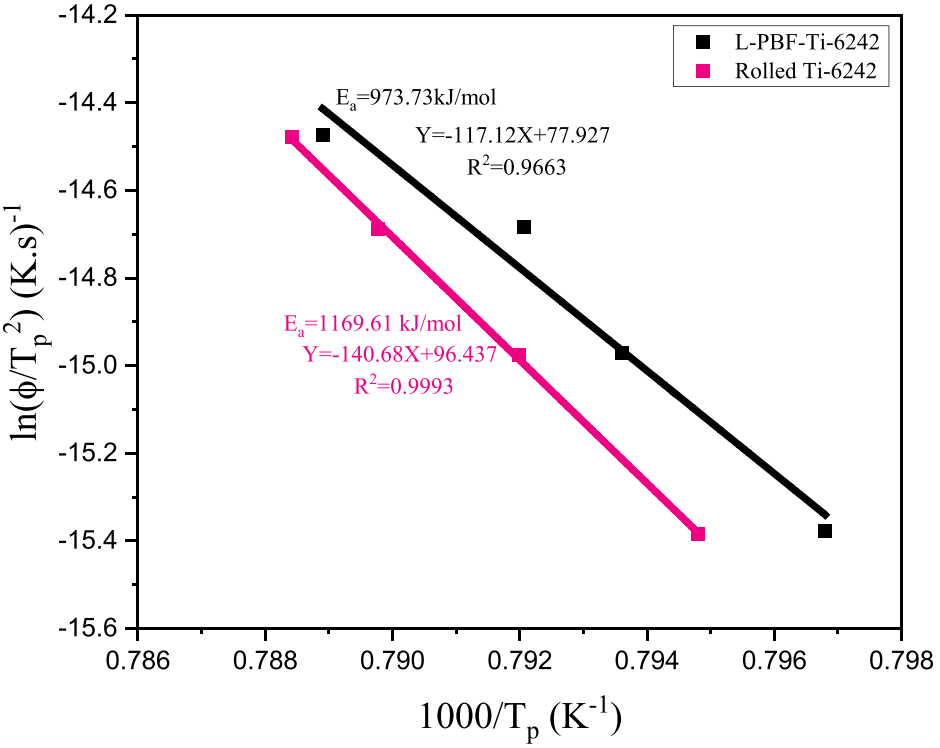

Fig. 3. Comparative activation energy study between rolled and L-PBF-Ti-6242.

kinetics due to higher Ti-64-G5 content (higher oxygen content) in some positions and keeping the kinetics similar to Ti-64-G23 in the positions which has a lower percentage of Ti-64-G5 comparative to Ti-64-G23. This heterogeneous distribution of Ti-64-G5 in Ti-64-MG (means heterogeneous distribution of oxygen in Ti-64-MG) delays the transformation kinetics in Ti-64-MG. Considering the same reason, L-PBF-Ti-64-MG possesses a higher α to β transformation activation energy compared to L-PBF-Ti-64-G23 (Fig. 2). It should be noted that unlike the electron beam melted (EBM)-Ti-64 where oxygen pickup throughout the process is a major issue [58,59], in the L-PBF-Ti-64 minimal oxygen pickup (in the order of ppm) may occur [34]. The results in Ref. [34] were obtained by printing the samples using the same

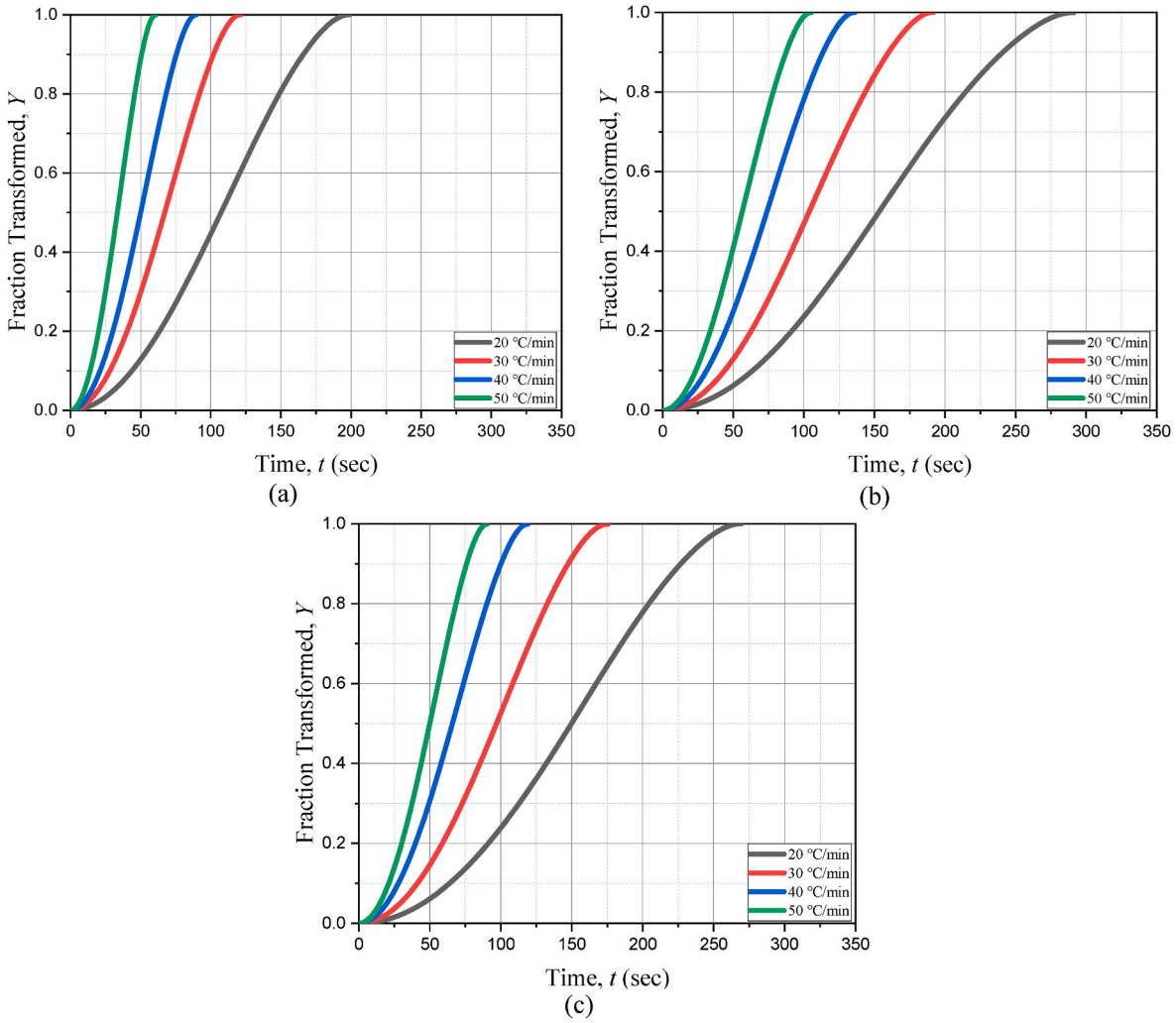

Fig. 4. Calculated fraction transformed (α to β) as a function of time for (a) L-PBF-Ti-6242, (b) L-PBF-Ti-64-MG, and (c) L-PBF-Ti-64-G23.

machine in this study. As a result, the oxygen content of the material will remain within the standard tolerance and will not affect the kinetic results significantly.

The speed of fraction transformed for both L-PBF-Ti-64 grades cannot be compared with L-PBF-Ti-6242 as Ti-6242 possesses a different chemical composition. On the other hand, by plotting the fraction transformed as a function of temperature, as seen in Fig. 5, it can be easily observed that L-PBF-Ti-64-G23 finishes the transformation at a lower temperature for the same heating rates because of the comparatively high β stabilizing elements. The transformation in L-PBF-Ti-64-MG and L-PBF-Ti-6242 finishes at higher temperatures. As explained earlier, this is due to the heterogeneous distribution of oxygen in L-PBF-Ti-64-MG which delays the transformation kinetics and availability of less β stabilizing element in L-PBF-Ti-6242 as it is a near α alloy. Fig. 5 also validates the thermodynamics concept discussed in section 3.1 that the higher the heating rate, the higher will be the temperature at which the transformation finishes.

3.4. Non-isothermal phase transformation kinetics

The non-isothermal phase transformation kinetics is investigated by employing the modified Johnson-Mehl-Avrami-Kolmogorov (JMAK) model. The JMAK model is a common approach to analyzing the isothermal phase transformation kinetics [60–64]. The solution of the JMAK model assuming a time-independent nucleation and growth rates for isothermal heating is represented by Eq. (3) [65]:

$$Y = 1 - \exp\left[-(kt)^n\right] \tag{3}$$

where Y is the fraction transformed at a given time (t) after the transformation start, n is the Avrami exponent and k is the overall rate constant which is a function of temperature. Since the JMAK model is valid for isothermal transformation conditions it has been modified for non-isothermal transformation by substituting the expression for k in Eq. (3) with a temperature-dependent term as follows [40,41,66]:

$$k(T) = k_0 \, exp\left(-\frac{E_a}{RT}\right) \tag{4}$$

where k_0 is the pre-exponential factor. The activation energy (E_a) could be evaluated through the Kissinger model (Eq. (1)). The general JMAK equation can be then rewritten as:

$$Y = 1 - exp\left\{-\left[\int_{t_o}^{t} k(T)dt\right]^n\right\} \tag{5}$$

where t_0 is the transformation start time. For a constant value of temperature, Eq. (5) is the general form of the JMAK model, however, for continuous heating at a constant rate of $\varphi = \frac{dT}{dt}$, Eq. (5) is revised as follows [40,41,66]:

$$Y = 1 - \exp\left[-\left\{\left(\frac{1}{\Phi}\right)\int_{T_o}^{T} k(T)dT\right\}^n\right] \tag{6}$$

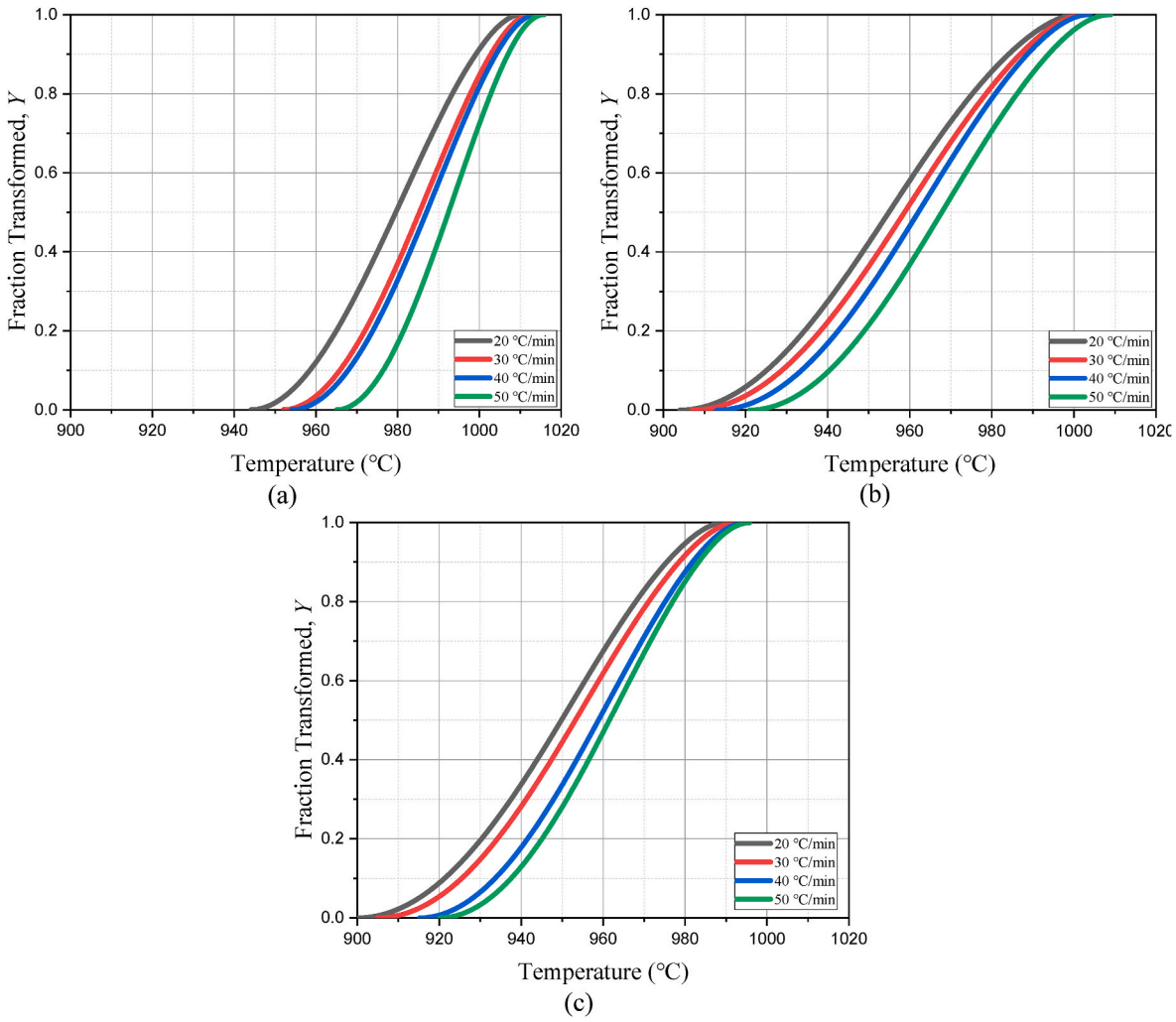

Fig. 5. Calculated fraction transformed (α to β) as a function of temperature, (a) L-PBF-Ti-6242, (b) L-PBF-Ti-64-MG, and (c) L-PBF-Ti-64-G23.

By substituting the expression of k from Eq. (4), the modified expression to model non-isothermal phase transformation kinetics for a constant heating rate at any given temperature T (K) is expressed as follows [42, 52]:

$$Y = 1 - exp\left[- \left\{ \frac{k_0}{\Phi} \left(exp \frac{-E_a}{RT} \right) (T - T_o) \right\}^n \right] \tag{7}$$

where Φ is the heating rate (K/sec or °C/s), T_o is the onset temperature of the phase transformation (in K) that can be determined from the DSC curves, and R is the universal gas constant (8.314 J/mol.K). The value of n and k_0 was calculated by performing a curve fitting to the experimental transformed fraction curves (obtained from the DSC experiments) using the solver tool of MS Excel. The fitting was done for each heating rate and the final curve was made using the average n and k_0 values as shown in Table 4 along with respective activation energies. The value of n can be correlated to the nucleation rate [67]. The comparison between the n-value for the L-PBF-Ti-64-MG and L-PBF-Ti-64-G23 shows that the former possesses a lower Avrami exponent. Such a difference shows that the nucleation rate is lower in the L-PBF-Ti-64-MG. As discussed previously, the lower nucleation rate is associated with the heterogenous oxygen distribution in the chemistry of the L-PBF-Ti-64-MG.

Table 4
Avrami exponent, pre-exponential factor, and activation energy for L-PBF-Ti-6242, L-PBF-Ti-64-MG, and L-PBF-Ti-64-G23.

	L-PBF-Ti-6242	L-PBF-Ti-64-MG	L-PBF-Ti-64-G23
n	0.75	0.59	0.68
k_0	2.55×10^{38}	4.56×10^{32}	3.75×10^{30}
E_a (kJ/mol)	937.73	824.61	770.18

In the next step, these values were used to predict the α to β fraction transformed. Both the experimental and calculated (predicted) fraction transformed curves for all the heating rates are shown in Fig. 6. It is seen that a good fit is achieved between the experimental and calculated data, which validates the kinetics models developed in this study.

To further analyze the phase transformation kinetics and characteristics, the local Avrami exponent (n) was evaluated using Eq. (8) [42]:

$$n = \frac{1}{1 + \frac{E_a}{RT}\left(1 - \frac{T_o}{T}\right)} \frac{d[ln\{-ln(1-Y)\}]}{d\left[ln\left(\frac{T-T_o}{\varphi}\right)\right]} \tag{8}$$

The slope of $ln[-ln(1-Y)]$ versus $ln\left(\frac{T-T_o}{\varphi}\right)$ plot indicates the variation of n throughout the transformation process. The local n is an important parameter in solid-state phase transformation as it elaborates on the nucleation and growth mechanisms [67]. The heating rate of 20 °C/min was considered as an example to evaluate local n and the plots of $ln[-ln(1-Y)]$ versus $ln\left(\frac{T-T_o}{\varphi}\right)$ are shown in Fig. 7. The slope remains almost constant over the majority of the process. Such a characteristic could imply that the nucleation and growth behavior remains almost the same for a major part of the transformation in all three alloys. The value of local n was calculated as a function of the fraction transformed using

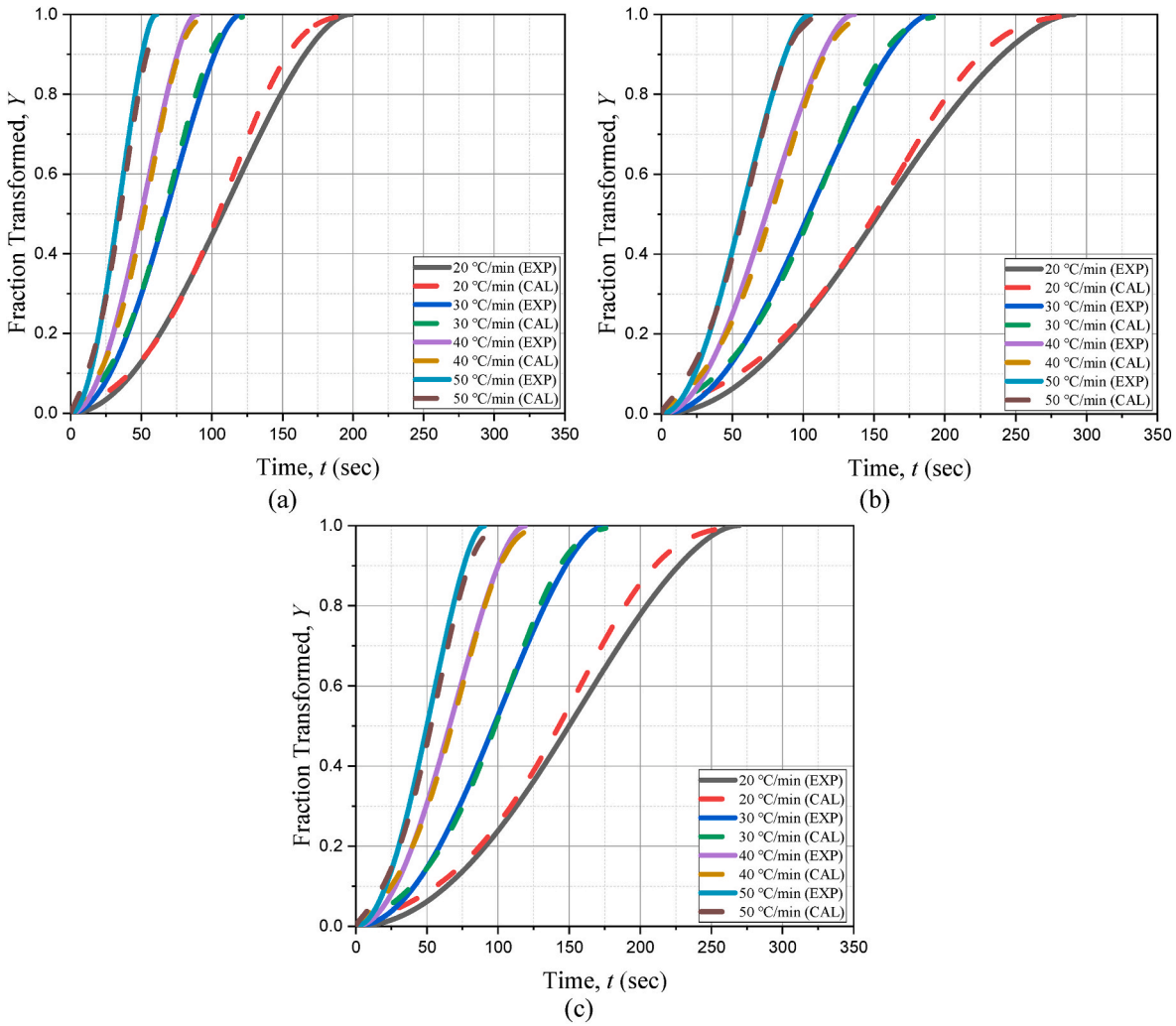

Fig. 6. Experimental and calculated non-isothermal fraction transformation comparison for (a) L-PBF-Ti-6242, (b) L-PBF-Ti-64-MG, and (c) L-PBF-Ti-64-G23.

Eq. (8) and the results are shown in Fig. 8. It is clear from Fig. 8 that the local n is almost constant for a major part of transformation (stage II) which validates the outcome of Fig. 7. The transformation process can be divided into three stages based on the value of local n as shown in Fig. 8. Stage I is associated with $0 < Y \leq 0.1$ where the value of local n is high once the system achieves activation energy, showing a high nucleation rate in the beginning of the process. As the process proceeds, the value of local n rapidly decreases indicating the reduction in nucleation rate [67]. In stage II, where $0.1 < Y \leq 0.95$, the nucleation rate slowly goes down as the local n value decreases gradually. Such a trend indicates that in stage II the transformation proceeds only by the interface growth of all the nuclei generated in stage I with limited new nuclei formed [20]. This is due to the consumption of β stabilizing elements for the growth of the β phase resulting in a continuous drop in available β stabilizing elements [20]. The nucleation rate is limited because the elemental concentration of β stabilizing elements required for nucleation became less than the critical concentration [20,67]. In stage III for $Y > 0.95$, the kinetics is accelerated rapidly, and this abnormal behavior was observed in previous studies as well, but to the best of our knowledge, the reason is not yet clear [20,66].

An interesting outcome from Fig. 8 is the fact that for a major portion of transformation (stage II) the value of local n is close to the constant value of n obtained from the solver shown in Table 4, confirming the validation of the developed model for all the alloys studied in this work.

3.5. Isothermal phase transformation kinetics

The validity of the calculated values of kinetic parameters E_a, n, and k_0 is proven, as the modified JMAK model for all three alloys in this work was validated by a good agreement between the experimental and calculated data for non-isothermal transformation. Further, these values can be used to calculate the fraction transformation ratio as a function of time for isothermal holding using Eqs. (3) and (4) [57]. By substituting the value of E_a, and k_0 in Eq. (4) the respective value of k for a constant temperature is determined. Futher, using the obtained value of k and n in Eq. (3), the frcation transformation is calculated for that constant temperature with varying time (t) [57].

The study of isothermal phase transformation kinetics is important to quantify the β phase in the α matrix during isothermal heat treatment. Previous studies on the L-PBF-Ti-6242 showed the formation of ultrafine α' microstructure due to rapid cooling, resulting in high strength in the as-built condition [16,38]. The traditional route of heat treatment, which consists of solutionizing followed by aging, coarsens the microstructure which deteriorates the mechanical properties [68]. On the other hand, direct aging is a better route for strengthening. The formation of nano-β precipitates after aging strengthens the material by the principle of precipitation hardening [69]. Rieger et al. [16] studied the effect of stress relief annealing (SRA) on the L-PBF-Ti-6242 and showed that the SRA at 800–850°C for 1–3 h caused the formation of β precipitates participating in the strength enhancement. These nano-β particles hinder the dislocation motion which results in higher strength by

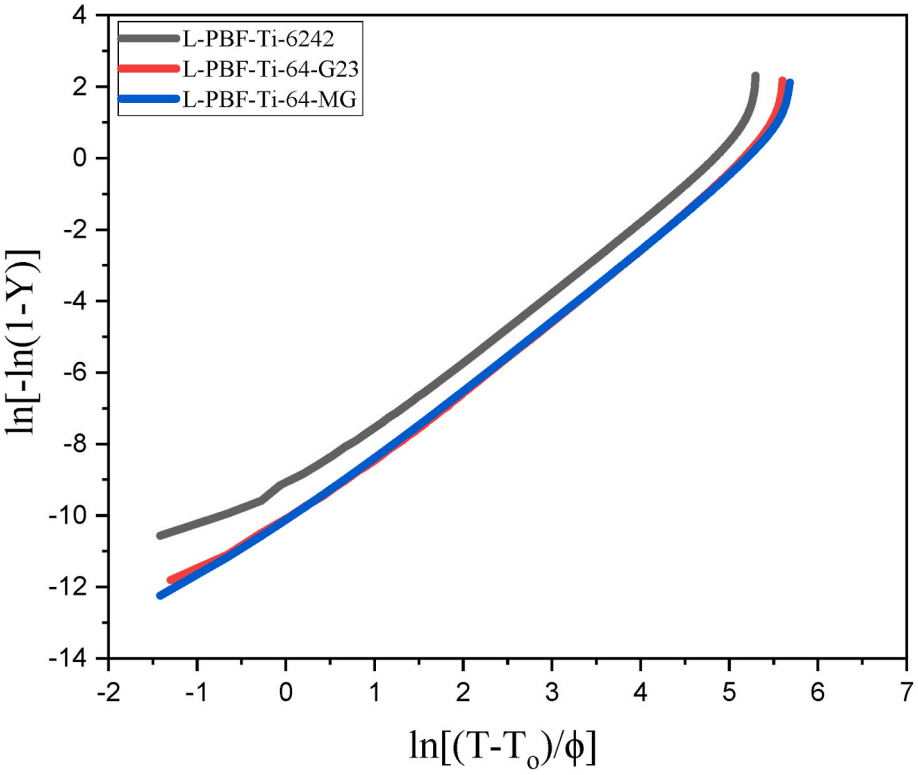

Fig. 7. Plot of $ln[-ln(1-Y)]$ versus $ln\left(\frac{T-T_o}{\varphi}\right)$ for L-PBF-Ti-6242, L-PBF-Ti-64-G23 and L-PBF-Ti-64-MG.

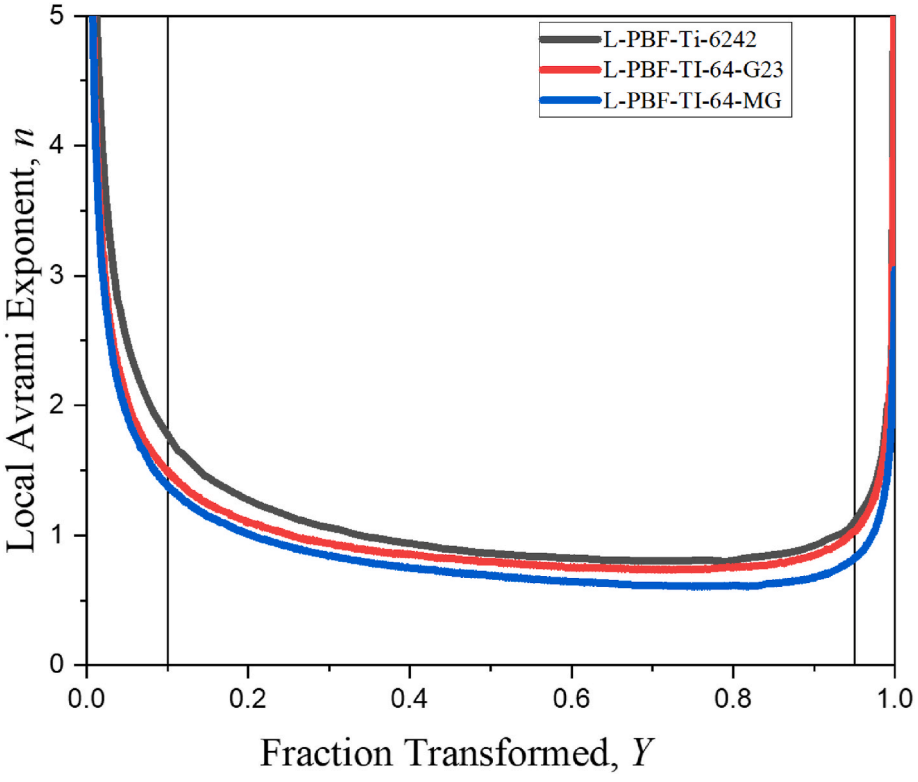

Fig. 8. Variation in local Avrami exponent versus fraction transformed for L-PBF-Ti-6242, L-PBF-Ti-64-G23, and L-PBF-Ti-64-MG.

compromising the ductility [38]. Based on the previous studies, the L-PBF-Ti-6242 demands a balance between nanotwins and β precipitates in the α matrix. The nanotwins in the as-built microstructure accommodate the dislocations which enhance the ductility of the material. These nanotwins are annihilated by aging at 595 °C for 8 h [38]. On the other hand, aging is necessary for enough β precipitate formation to enhance the strength [16]. Similarly, the aging parameter of the L-PBF-Ti-64 should be chosen carefully as over-aging lowers the strength

and fracture toughness by coarsening the fine as-built α' grains [70,71]. Therefore, it is necessary to develop kinetics models for the isothermal heat treatments of titanium alloys.

The isothermal heat treatment was studied at 1050, 1000, 950, and 900 °C. These temperatures were selected based on the onset and peak temperatures of the phase transformation extracted from the DSC curves. The transformation curves for isothermal heat treatment at respective temperatures are shown in Fig. 9. Similar to the trend observed for the non-isothermal phase transformations, the isothermal phase transformation is faster in the L-PBF-Ti64-G23, compared to the L-PBF-Ti64-MG. The reason is the homogeneity of the oxygen content. Moreover, for all three alloys, the transformation is faster at higher temperatures, however, for a better understanding and comparison of transformation kinetics, the rate of phase transformation is calculated.

Table 5. compares the rate of phase transformation for isothermal holding at different temperatures shown in Fig. 9. The rate of phase transformation is calculated as the inverse of the time required for 50% of the transformation ($t_{0.5}$) and represented as $r = \frac{1}{t_{0.5}}$. A higher value of r implies higher transformation kinetics.

It is clear from Table 5 that at a higher temperature (1050°C) the transformation rate is faster for all three alloys. This represents the faster kinetics at higher temperatures which is an obvious phenomenon. On the other hand, the transformation kinetics of L-PBF-Ti-6242 is slower than L-PBF-Ti-64-MG and L-PBF-Ti-64-G23 at respective temperatures. This is obvious as L-PBF-Ti-6242 is a near α titanium alloy with little β stabilizer. Similarly, comparing L-PBF-Ti-64-MG and L-PBF-Ti-64-G23 the inhomogeneity of oxygen delays the kinetics in L-PBF-Ti-64-MG resulting smaller value of the rate of phase transformation. For both isothermal holding and continuous heating, L-PBF-Ti-6242 has the slowest rate of phase transformation followed by L-PBF-Ti-64-MG.

Table 5
The rate of phase transformation at different holding temperatures.

Temperature (°C)	L-PBF-Ti-6242	L-PBF-Ti-64-MG	L-PBF-Ti-64-G23
	r (s^{-1})		
1050	1.47	2.31	2.48
1000	0.05	0.12	0.15
950	1.06×10^{-3}	5.05×10^{-3}	8.06×10^{-3}
900	1.79×10^{-5}	1.61×10^{-4}	3.21×10^{-4}

3.6. Effect of initial microstructure on phase transformation kinetics

The rate of phase transformation depends both on the heating rate and the initial microstructure. As discussed in section 3.3, the rate of transformation highly depends on the heating rate, the higher the heating rate the higher will be the transformation kinetics. In addition, the initial microstructure can alter the phase transformation kinetics. An important aspect of the microstructures of the AM titanium alloys is their metastable and hierarchical characteristics. The microstructure of AM titanium alloys (specifically the L-PBF alloys) consists of a fine lath

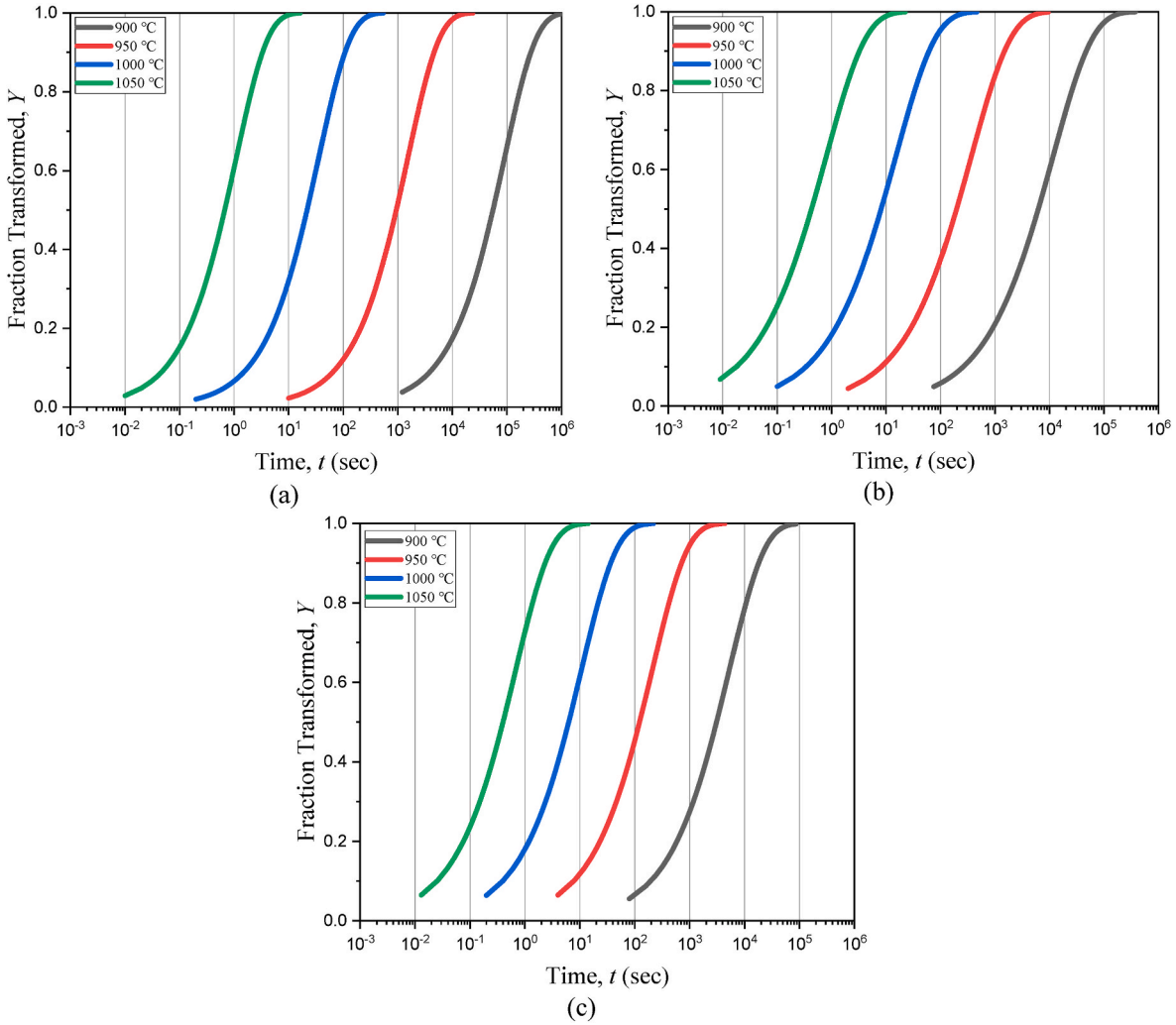

Fig. 9. Calculated isothermal fraction transformed (α to β) as a function of time, (a) L-PBF Ti-6242, (b) L-PBF-Ti-64 MG, and (c) L-PBF-Ti-64-G23.

martensitic α'/α structure [72], featured by nanotwins within the martensites [1], and the network of entangled dislocations [73]. To assess the role of the initial microstructure in the α to β transformation kinetics, a sample of L-PBF-Ti-6242 was analyzed using the DSC under ten consecutive heating cycles. The sample was heated to 1200 °C with a heating rate of 20 °C/min and then cooled down to 50 °C under a slow cooling rate, followed by the same heating and cooling patterns for 10 cycles. Thermal cycles of 2 to 10 gradually altered the microstructure of the material toward an equilibrium state. Therefore, it is expected that the phase transformation kinetics is different at different cycles.

Fig. 10 shows the SEM microstructure of as-built L-PBF-Ti-6242 along with the microstructure of the material after 4 cycles and 9 cycles of DSC. These two microstructures represent the starting microstructure for the 5th and 10th cycles, respectively. As seen, the microstructure of the as-built L-PBF-Ti-6242 consists of an acicular martensitic α'/α structure which is a common structure in the as-built L-PBF-Ti-6242 [16,38]. After 4 cycles of heating and cooling, the β phase developed along the α'/α boundaries and the α'/α lath grew [39]. At the end of the 9th cycle, coarser α'/α laths developed in the material. As a result, the starting microstructure for the 1st, 5th, and 10th DSC cycles are different.

Fig. 11 shows the fraction transformed as a function of $\frac{t}{t^*}$ where t^* is the time required to complete the α to β transformation in the 1st cycle that represents the transformation kinetics of L-PBF-Ti-6242 with as-built or initial microstructure. It is observed from Fig. 11 that the time required for α to β transformation in the 5th and 10th heating cycles is ~1.1 and ~1.2 times of the 1st heating cycle, respectively. The reason for the increase in transformation time with each heating cycle would be the change in microstructure after every cycle which results in a new initial microstructure at the beginning of every heating cycle (Fig. 10). Fan. et al. [21] discussed the effect of initial microstructure in the transformation kinetics of TA15 titanium alloy, another near α alloy, and showed that the rate of phase transformation is different for different initial microstructures as it changes from equiaxed α to lamellar α. In the current study, the initial microstructure was martensitic α'/α, due to rapid cooling during the L-PBF process [16,38]. The microstructural features gradually changed and α'/α coarsened after the completion of each heating and cooling cycle. As a result, each cycle started with a different microstructure. Referring to Fig. 11, altering the as-built microstructure and eliminating the hierarchical features resulted in a slower α to β transformation kinetics. It appears that the ultrafine and hierarchical microstructural features can potentially expedite the process of transformation. Therefore, these features can be used to develop a proper heat treatment process and tailor the desired microstructure to obtain both strength and ductility simultaneously.

3.7. Design of heat treatment based on phase transformation kinetics results

A major issue associated with the mechanical properties of L-PBF titanium alloys (including both Ti-64 and Ti-6242) is their low ductility in the as-built condition. To overcome such a shortcoming, the as-built samples are heat treated. Some efforts have been made to design both subtransus and supertransus heat treatments for L-PBF-Ti-6242 to improve ductility [16,38,39,74]. These heat treatments mainly were developed based on the available heat treatments for Ti-64 alloy. In addition, it appears that finding the optimum heat treatment conditions for L-PBF-Ti-6242 to obtain the desired microstructure heavily relies on trial and error. Moreover, in most of the available heat treatments, the material is exposed to high temperatures for a long time. As a result, the ultrafine and hierarchical characteristics of the microstructure will be annihilated.

In this paper, the results of the kinetics modeling were employed to design a two-step heat treatment procedure. The philosophy behind such a heat treatment design was to promote the nucleation of the β phase over a short hold at a subtransus temperature followed by a long hold at a temperature below 595°C to preserve the hierarchical characteristics of the microstructure, and in specific the nanotwins (see Fig. 1 (a), the nanotwin annihilation peak). Referring to the isothermal kinetics modeling results presented in Fig. 9, holding the L-PBF-Ti-6242 at 900°C for 10 min will allow for less than 10% β transformation. Therefore, the first step of the heat treatment was designed as 10 min of holding at 900°C followed by water quenching (designated as 900°C-10min). In this step, nuclei of β can form by local diffusion of the β stabilizing element (*i.e.* Mo). It should be mentioned that despite water quenching the sample, a portion of β will transform to α/α' since Ti-6242 is a near-α alloy. In the next step, the sample was aged at 300°C for 48 h (designated as 900°C-10min/300°C-48hr) to promote the growth of β

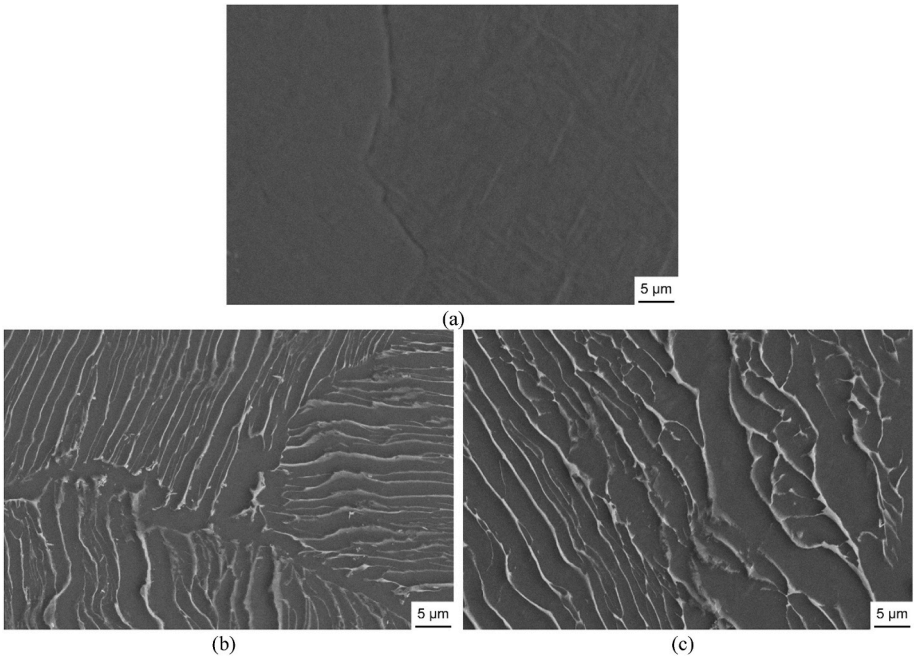

Fig. 10. SEM images of (a) as-built L-PBF-Ti-6242 and L-PBF-Ti-6242 after (b) 4 cycles and (c) 9 cycles of DSC. The dark phase is α/α' and the bright phase is α+β.

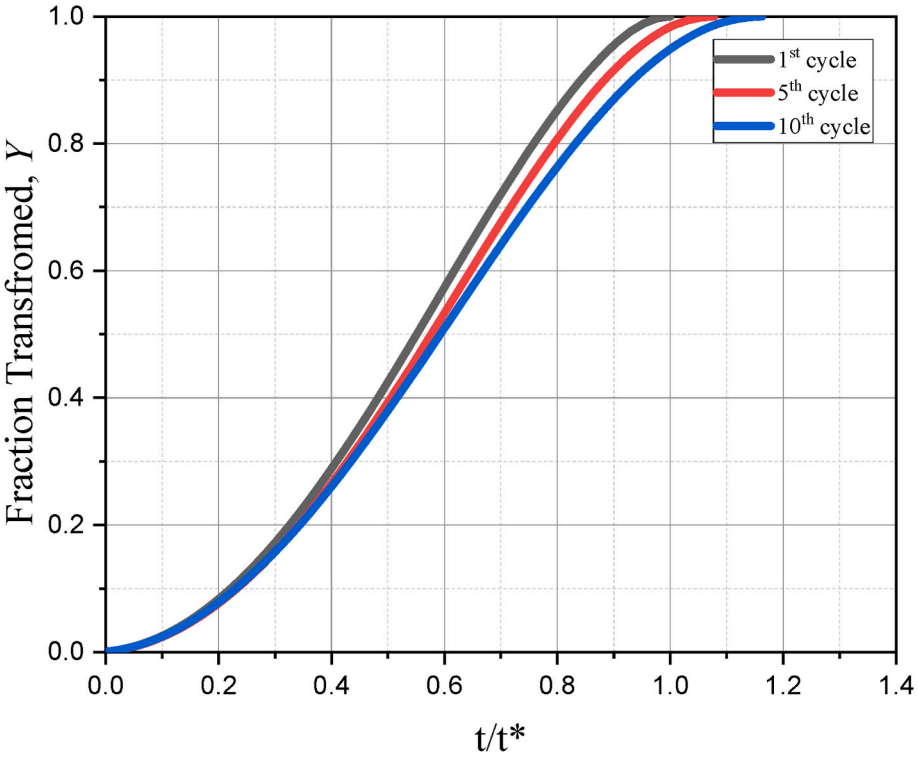

Fig. 11. Calculated fraction transformed (α to β) as a function of time for ten continuous heating cycles of L-PBF-Ti-6242 at a heating rate of 20 °C/min. t^* denotes the required time for completion of α to β phase transformation in the as-built L-PBF-Ti-6242.

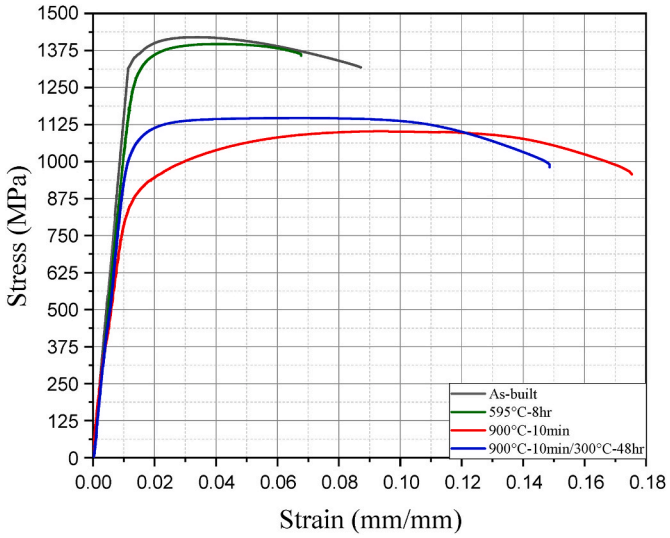

Fig. 12. Tensile properties of as-built and heat-treated L-PBF-Ti6242.

nuclei. One sample was also heat treated using the common 595°C-8hr for comparison. Fig. 12 shows the resulting tensile properties and Fig. 13 shows the corresponding microstructures.

As seen in Fig. 12, the as-built L-PBF-Ti-6242 possesses a tensile strength (σ_{UTS}) and strain at fraction (ε_f) of 1420 MPa and 8.7%, respectively. The high strength of the as-built sample is due to the acicular martensitic α/α' structure as seen in Fig. 13 (a). The common 595°C-8hr treatment decreased both σ_{UTS} and ε_f to 1397 MPa and 6.6%, respectively. The main reason for such a detrimental effect is the substantial changes in the microstructure as seen in Fig. 13 (b). This heat treatment decomposed the α/α' structure into dispersed β particles. The short holding at 900°C for 10 min decreased σ_{UTS} to 1102 MPa, however ε_f substantially enhanced to 17.5%. As seen in Figs. 13 (c), 10 min of holding at 900°C resulted in the evolution of the β phase over the lath martensite boundaries along with the nucleation of nanoscaled β within the laths. By aging this sample at 300°C for 48hr, the nanoscaled β grew with a lamellar morphology, which resulted in the improvement of strength (σ_{UTS} = 1147 MPa) with minimal effect on ductility loss (ε_f = 14.7%).

While this part of the study proves the importance and efficiency of the kinetics models to design the proper heat treatments for L-PBF titanium alloys, it should be noted that this effort is still ongoing. In our future studies, we will explore microstructures using advanced microscopy techniques and correlate them to mechanical properties.

4. Conclusions

In the current study, the α to β phase transformation kinetics of Ti-6242 and two grades of Ti-64 titanium alloys fabricated through L-PBF were investigated using DSC under different heating rates. The difference between the two grades of Ti64 was the homogeneity of oxygen distribution in the powder feedstock. The activation energy was evaluated through the Kissinger model and the modified JMAK equation was employed to develop the kinetics models for both non-isothermal and isothermal transformations. The conclusions of the study are as follows:

- The characteristics of the α to β phase transformation (including the onset, peak, and end temperatures) were different between the three alloys. L-PBF-Ti-6242 possessed the highest peak temperature due to the stability of the α phase. On the other hand, the heterogeneous distribution of the oxygen content in L-PBF-Ti64-MG shifted the peak temperature to higher values compared to the L-PBF-Ti64-G23.
- L-PBF-Ti-6242 had the highest α to β transformation activation energy of 973.73 kJ/mol compared to 824.61 and 770.18 kJ/mol for L-PBF-Ti64-MG and L-PBF-Ti64-G23, respectively. The comparatively high value of activation energy of L-PBF-Ti-6242 was the result of

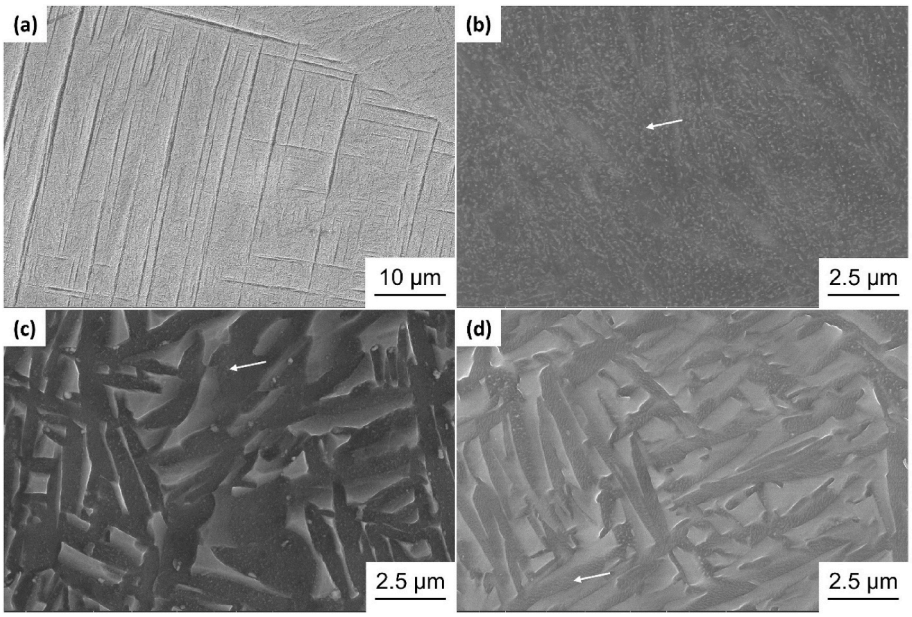

Fig. 13. SEM images of (a) as-built, (b) 595°C-8hr, (c) 900°C-10min, and (d) 900°C-10min/300°C-48hr L-PBF-Ti-6242 samples. The white arrows show the inter-lath, β particles.

less β stabilizing element available in its composition. The difference between the two grades of the L-PBF-Ti64 was also a result of oxygen homogeneity.

- Comparing the two grades of L-PBF-Ti-64 investigated for isothermal transformation, the heterogeneous distribution of oxygen in L-PBF-Ti-64-MG delayed the kinetics. Such a characteristic resulted in comparatively slower transformation kinetics for L-PBF-Ti-64-MG than L-PBF-Ti-64-G23.
- The DSC results of ten continuous heating and cooling cycles of L-PBF-Ti-6242 showed that the phase transformation kinetics depends on the initial microstructure, where the as-built hierarchical and metastable microstructure expedited the phase transformation kinetics. Such behavior is important since it implies the importance of the as-built microstructure in designing the heat treatments and engineering the desired microstructures.
- The kinetics models were employed to design a two-step heat treatment for L-PBF-Ti-6242 to improve its ductility with minimal effect on strength. 10 min of holding at 900°C followed by aging at 300°C for 48 h resulted in an increase in the ductility from 8.7% in the as-built condition to 14.7% after heat treatment. Meanwhile, the strength exhibited a slight reduction from 1420 MPa to 1147 MPa. Such changes were correlated to the microstructure of the material, as the nanoscaled β phase nucleated at 900°C and grew at 300°C, while the other hierarchical features were preserved.

CRediT authorship contribution statement

Harish Chandra Kaushik: Methodology, Validation, Investigation, Writing – original draft. **Mahdi Habibnejad Korayem:** Conceptualization, Writing – review & editing. **Amir Hadadzadeh:** Conceptualization, Methodology, Validation, Investigation, Resources, Writing – review & editing, Supervision.

Declaration of competing interest

The authors declare that they have no known competing financial interests or personal relationships that could have appeared to influence the work reported in this paper.

Data availability

The data that has been used is confidential.

Acknowledgment

The authors would like to acknowledge Dr. Fotovvati and Dr. Asadi at the Metal Additive Manufacturing Laboratory at the University of Memphis for facilitating the fabrication of the L-PBF components.

References

[1] M.J. Donachie, Introduction to selection of titanium alloys, Titanium (2021) 5–11, https://doi.org/10.31399/asm.tb.ttg2.t61120005.
[2] D. Eylon, S. Fujishiro, F.H. Froes, Titanium alloys for high temperature applications — a review, High Temp. Mater. Process. 6 (1984) 81–92, https://doi.org/10.1515/HTMP.1984.6.1-2.81.
[3] J. Mezzetta, Process-Property Relationships of Ti6Al4V Fabricated through Selective Laser Melting, Department of Mining and Materials Engineering, McGill University, Montreal, Quebec, 2016. Master's Thesis.
[4] S. Oh, K. Woo, J. Kim, S. Kwak, The effect of Al and V on microstructure and transformation of β phase during solution treatments of cast Ti-6Al-4V alloy, Korean J. Met. Mater. 55 (2017) 18–20, https://doi.org/10.3365/kjmm.2017.55.3.150.
[5] A.S.M. International, Heat treating processes and related technology introduction, Heat Treater's Guide: Practices and Procedures for Irons and Steels, 1995.
[6] B. Sefer, R. Gaddam, J.J. Roa, A. Mateo, M.L. Antti, R. Pederson, Chemical milling effect on the low cycle fatigue properties of cast Ti–6Al–2Sn–4Zr–2Mo alloy, Int. J. Fatig. 92 (2016) 193–202, https://doi.org/10.1016/j.ijfatigue.2016.07.003.
[7] P.J. Postans, F.H. Froes, High temperature titanium alloys-A review, JOM 36 (1984) 55–62, https://doi.org/10.1007/BF03338617.
[8] J.B. Borradaile, R.H. Jeal, Critical Review-Mechanical Properties of Titanium Alloys, Rolls-Royce Ltd., Aero division, Derby, England, 1981.
[9] R.R. Boyer, An overview on the use of titanium in the aerospace industry, Mater. Sci. Eng. A. 213 (1996) 103–114, https://doi.org/10.1016/0921-5093(96)10233-1.
[10] A.K. Gogia, High-temperature titanium alloys, Defence Sci. J. 55 (2017) 149–179, https://doi.org/10.14429/dsj.55.1979.
[11] P. Homporová, C. Poletti, M. Stockinger, F. Warchomicka, Dynamic phase evolution in titanium alloy Ti-6A1-4V, Ti 2011 -, Proc. 12th World Conf. Titan. 1 (2012) 737–740.
[12] Z.C. Xu, H.P. Kriegel, The martensitic transformation in Ti-6Al-4V, Mater. Sci. Forum 914 (2018) 140–148. https://doi.org/10.4028/www.scientific.net/MSF.914.140.
[13] G. Steedman, S.F. Corbin, Determining sintering mechanisms and rate of in situ homogenisation during master alloy sintering of Ti6Al4V, Powder Metall. 58 (2015) 67–80, https://doi.org/10.1179/1743290114Y.0000000110.
[14] P.B. Vila, Effect of Heat Treatments on the Microstructure of Ti-6Al-4V, Vienna University of Technology, 2010. Master's thesis.

[15] Z. Li, C. Liu, B. Wang, C. Wang, Z. Wang, F. Yang, C. Gao, H. Liu, Y. Qin, J. Wang, Heat treatment effect on the mechanical properties, roughness and bone ingrowth capacity of 3D printing porous titanium alloy, RSC Adv. 8 (2018) 12471–12483, https://doi.org/10.1039/C7RA13313H.

[16] C. Fleißner-Rieger, T. Pfeifer, T. Jörg, T. Kremmer, M. Brabetz, H. Clemens, S. Mayer, Selective laser melting of a near-α Ti6242S alloy for high-performance automotive parts, Adv. Eng. Mater. 23 (2021), 2001194, https://doi.org/10.1002/adem.202001194.

[17] H. Galarraga, R.J. Warren, D.A. Lados, R.R. Dehoff, M.M. Kirka, P. Nandwana, Effects of heat treatments on microstructure and properties of Ti-6Al-4V ELI alloy fabricated by electron beam melting (EBM), Mater. Sci. Eng. A. 685 (2017) 417–428, https://doi.org/10.1016/j.msea.2017.01.019.

[18] P. Yadav, K.K. Saxena, Effect of heat-treatment on microstructure and mechanical properties of Ti alloys: an overview, Mater. Today Proc. 26 (2019) 2546–2557, https://doi.org/10.1016/j.matpr.2020.02.541.

[19] S. Malinov, Z. Guo, W. Sha, A. Wilson, Differential scanning calorimetry study and computer modeling of β ⇒ α phase transformation in a Ti-6Al-4V alloy, Metall. Mater. Trans. A Phys. Metall. Mater. Sci. 32 (2001) 879–887, https://doi.org/10.1007/s11661-001-0345-x.

[20] H. Yu, W. Li, H. Zou, S. Li, T. Zhai, L. Liu, Study on non-isothermal transformation of Ti-6Al-4V in solution heating stage, Metals 9 (2019) 968, https://doi.org/10.3390/met9090968.

[21] X. Fan, Q. Li, A. Zhao, Y. Shi, W. Mei, The effect of initial structure on phase transformation in continuous heating of a TA15 titanium alloy, Metals 7 (2017), https://doi.org/10.3390/met7060200.

[22] Xin Li , Qisong Zhu , Sinong Liu , Feng Li , Fuwen Chen , Hui Wang , Hui Chang, Phase transformation and microstructure evolution of Ti6Al4V-0.55Fe alloy with different initial microstructure during continuous heating, J. Mater. Res. Technol. (IF 6.267)Pub Date: 2022-03-19 , DOI:10.1016/j.jmrt.2022.03.093.

[23] M. Peters, C. Leyens, Fabrication of titanium alloys, Titan. Titan. Alloy (2005) 245–261, https://doi.org/10.1002/3527602119.ch8.

[24] J. Gussone, K. Bugelnig, P. Barriobero-Vila, J.C. da Silva, U. Hecht, C. Dresbach, F. Sket, P. Cloetens, A. Stark, N. Schell, J. Haubrich, G. Requena, Ultrafine eutectic Ti-Fe-based alloys processed by additive manufacturing – a new candidate for high temperature applications, Appl. Mater. Today 20 (2020), 100767, https://doi.org/10.1016/j.apmt.2020.100767.

[25] Y.M. Wang, T. Voisin, J.T. McKeown, J. Ye, N.P. Calta, Z. Li, Z. Zeng, Y. Zhang, W. Chen, T.T. Roehling, R.T. Ott, M.K. Santala, P.J. Depond, M.J. Matthews, A. V. Hamza, T. Zhu, Additively manufactured hierarchical stainless steels with high strength and ductility, Nat. Mater. 17 (2018) 63–70, https://doi.org/10.1038/NMAT5021.

[26] L. Liu, Q. Ding, Y. Zhong, J. Zou, J. Wu, Y.L. Chiu, J. Li, Z. Zhang, Q. Yu, Z. Shen, Dislocation network in additive manufactured steel breaks strength–ductility tradeoff, Mater, Today 21 (2018) 354–361, https://doi.org/10.1016/j.mattod.2017.11.004.

[27] A. Zafari, K. Xia, High Ductility in a fully martensitic microstructure: a paradox in a Ti alloy produced by selective laser melting, Mater. Res. Lett. 6 (2018) 627–633, https://doi.org/10.1080/21663831.2018.1525773.

[28] A. Hadadzadeh, C. Baxter, B.S. Amirkhiz, M. Mohammadi, Strengthening mechanisms in direct metal laser sintered AlSi10Mg: comparison between virgin and recycled powders, Addit. Manuf. 23 (2018) 108–120, https://doi.org/10.1016/j.addma.2018.07.014.

[29] A. Hadadzadeh, B.S. Amirkhiz, A. Odeshi, J. Li, M. Mohammadi, Role of hierarchical microstructure of additively manufactured AlSi10Mg on dynamic loading behavior, Addit. Manuf. 28 (2019) 1–13, https://doi.org/10.1016/j.addma.2019.04.012.

[30] H. Wang, Q. Chao, H.S. Chen, Z.B. Chen, S. Priming, W. Xu, S.P. Ringer, X.Z. Liao, Formation of a transition V-rich structure during the α' to α + β phase transformation process in additively manufactured Ti-6Al-4 V, Acta Mater. 235 (2022), 118104, https://doi.org/10.1016/j.actamat.2022.118104.

[31] R.H. Doremus, The role of dislocations in carbide precipitation in α-iron, Acta Metall. 6 (1958) 674–679, https://doi.org/10.1016/0001-6160(58)90058-0.

[32] U.K. Viswanathan, S. Banerjee, R. Krishnan, Effects of aging on the microstructure of 17-4 PH stainless steel, Mater. Sci. Eng. A 100 (1988) 181–189, https://doi.org/10.1016/0025-5416(88)90420-X.

[33] H. Wang, Z.G. Zhu, H. Chen, A.G. Wang, J.Q. Liu, H.W. Liu, R.K. Zheng, S.M.L. Nai, S. Primig, S.S. Babu, S.P. Ringer, X.Z. Liao, Effect of cyclic rapid thermal loadings on the microstructural evolution of a CrMnFeCoNi high-entropy alloy manufactured by selective laser melting, Acta Mater. 196 (2020) 609–625.

[34] B. Fotovvati, S.A. Etesami, E. Asadi, Process-property-geometry correlations for additively-manufactured Ti–6Al–4V sheets, Mater. Sci. Eng. A 760 (2019) 431–447, https://doi.org/10.1016/j.msea.2019.06.020.

[35] A. Hadadzadeh, B. Shalchi Amirkhiz, B. Langelier, J. Li, M. Mohammadi, Microstructural consistency in the additive manufactured metallic materials: a study on the laser powder bed fusion of AlSi10Mg, Addit. Manuf. 46 (2021), 102166, https://doi.org/10.1016/j.addma.2021.102166.

[36] B. Vrancken, L. Thijs, J.P. Kruth, J.V. Humbeeck, Heat treatment of Ti6Al4V produced by selective laser melting: microstructure and mechanical properties, J. Alloys Compd. 541 (2012) 177–185, https://doi.org/10.1016/j.jallcom.2012.07.022.

[37] A.M. Khorasani, I. Gibson, A. Ghaderi, M.I. Mohammed, Investigation on the effect of heat treatment and process parameters on the tensile behaviour of SLM Ti-6Al-4V parts, Int. J. Adv. Manuf. Technol. 101 (2019) 3183–3197, https://doi.org/10.1007/s00170-018-3162-8.

[38] H. Fan, S. Yang, Effects of direct aging on near-alpha Ti–6Al–2Sn–4Zr–2Mo (Ti-6242) titanium alloy fabricated by selective laser melting (SLM), Mater. Sci. Eng. A. 788 (2020), 139533, https://doi.org/10.1016/j.msea.2020.139533.

[39] Z. Zhu, F.L. Ng, H.L. Seet, S.M.L. Nai, Tailoring the microstructure and mechanical property of laser powder bed fusion fabricated Ti–6Al–2Sn–4Zr–2Mo via heat treatment, J. Alloys Compd. 895 (2022), 162648, https://doi.org/10.1016/j.jallcom.2021.162648.

[40] H. Li, K. Gai, L. He, C. Zhang, H. Cui, M. Li, Non-isothermal phase-transformation kinetics model for evaluating the austenization of 55CrMo steel based on Johnson-Mehl-Avrami equation, Mater. Des. 92 (2016) 731–741, https://doi.org/10.1016/j.matdes.2015.12.110.

[41] J. Torrens-Serra, S. Venkataraman, M. Stoica, U. Kuehn, S. Roth, J. Eckert, Non-isothermal kinetic analysis of the crystallization of metallic glasses using the master curve method, Materials 4 (2011) 2231–2243, https://doi.org/10.3390/ma4122231.

[42] T. Paul, A. Loganathan, A. Agarwal, S.P. Harimkar, Kinetics of isochronal crystallization in a Fe-based amorphous alloy, J. Alloys Compd. 753 (2018) 679–687, https://doi.org/10.1016/j.jallcom.2018.04.133.

[43] G. Lutjering, J.C. Williams, Titanium, Springer, 2007, https://doi.org/10.1007/978-3-540-73036-1.

[44] Z. Liu, G. Welsch, Effects of oxygen and heat treatment on the mechanical properties of alpha and beta titanium alloys, Metall. Mater. Trans. A 19 (1988) 527–542, https://doi.org/10.1007/BF02649267.

[45] C. Leyens, M. Peters, Titanium and Titanium Alloys: Fundamentals and Applications, John Wiley & Sons, 2003, https://doi.org/10.1002/3527602119.

[46] Hossein Eskandari Sabzi, Xiao-Hui Li, Chi Zhang, Hanwei Fu, David San-Martin, E. Pedro, J. Rivera-Diaz-del-Castillo, Deformation twinning-induced dynamic recrystallization during laser powder bed fusion, Scripta Mater. 207 (2022), 114307, https://doi.org/10.1016/j.scriptamat.2021.114307.

[47] K. Lu, L. Lu, S. Suresh, Strengthening materials by engineering coherent internal boundaries at the nanoscale, Science 324 (5925) (2009) 349–352, https://doi.org/10.1126/science.1159610.

[48] M.J. Donachie, Understanding the metallurgy of titanium, Titanium (2021) 13–24, https://doi.org/10.31399/asm.tb.ttg2.t61120013.

[49] D.G. Weldon, Differential scanning calorimetry, J. Prot. Coatings Linings 31 (2014) 21–23, https://doi.org/10.3139/9781569906446.007.

[50] W.F. Hemrninger, S.M. Sarge, The baseline construction and its influence on the measurement of heat with differential scanning calorimeters, J. Therm. Anal. 37 (1991) 1455–1477, https://doi.org/10.1007/bf01913481.

[51] X. Fu, X.D. Wang, B. Zhao, et al., Atomic-scale observation of non-classical nucleation-mediated phase transformation in a titanium alloy, Nat. Mater. 21 (2022) 290–296, https://doi.org/10.1038/s41563-021-01144-7.

[52] Y.H. Li, C. Yang, L.M. Kang, H.D. Zhao, S.G. Qu, X.Q. Li, W.W. Zhang, Y.Y. Li, Non-isothermal and isothermal crystallization kinetics and their effect on microstructure of sintered and crystallized TiNbZrTaSi bulk alloys, J. Non-Cryst. Solids 432 (2016) 440–452, https://doi.org/10.1016/j.jnoncrysol.2015.11.005.

[53] M. Carton, P. Jacques, N. Clément, J. Lecomte-Beckers, Study of transformations and microstructural modifications in Ti-LCB and Ti-555 alloys using differential scanning calorimetry, in: Proceedings of Ti-2007 Science and Technology, 2007, pp. 491–494. https://hdl.handle.net/2268/27540.

[54] Y.H. Wang, H. Kou, H. Chang, Z.S. Zhu, X.F. Su, J. Li, L. Zhou, Phase transformation in TC21 alloy during continuous heating, J. Alloys Compd. 472 (2009) 252–256, https://doi.org/10.1016/j.jallcom.2008.04.035.

[55] M.J. Starink, The determination of activation energy from linear heating rate experiments: a comparison of the accuracy of isoconversion methods, Thermochim. Acta 404 (2003) 163–176, https://doi.org/10.1016/S0040-6031(03)00144-8.

[56] H.E. Kissinger, Reaction kinetics in differential thermal analysis, Anal. Chem. 29 (1957) 1702–1706, https://doi.org/10.1021/ac60131a045.

[57] Z. Guo, W. Sha, D. Li, Quantification of phase transformation kinetics of 18 wt.% Ni C250 maraging steel, Mater. Sci. Eng. A. 373 (2004) 10–20, https://doi.org/10.1016/j.msea.2004.01.040.

[58] P. Nandwana, W.H. Peter, R.R. Dehoff, L.E. Lowe, M.M. Kirka, F. Medina, S. S. Babu, Recyclability study on Inconel 718 and Ti-6Al-4V powders for use in electron beam melting, Metall. Mater. Trans. B 47 (2015) 754–762, https://doi.org/10.1007/s11663-015-0477-9.

[59] W.J. Davids, H. Chen, K. Nomoto, H. Wang, S. Babu, S. Primig, X. Liao, A. Breen, S. P. Ringer, Phase transformation pathways in Ti-6Al-4V manufactured via electron beam powder bed fusion, Acta Mater. 215 (2021), 117131, https://doi.org/10.1016/j.actamat.2021.117131.

[60] M. Avrami, Kinetics of phase change. I: general theory, J. Chem. Phys. 7 (1939) 1103–1112, https://doi.org/10.1063/1.1750380.

[61] M. Avrami, Kinetics of phase change. II Transformation-time relations for random distribution of nuclei, J. Chem. Phys. 8 (1940) 212–224, https://doi.org/10.1063/1.1750631.

[62] M. Avrami, Granulation, phase change, and microstructure kinetics of phase change. III, J. Chem. Phys. 9 (1941) 177–184, https://doi.org/10.1063/1.1750872.

[63] W.A. Johnson, R.F. Mehl, Reaction kinetics in processes of nucleation and growth, T. Am. Inst. Min. Met. Eng. 135 (1939) 416–442.

[64] A.N. Kolmogorov, Selected Works of A.N. Kolmogorov. Volume2, Probability Theory and Mathematical Statistics, 1991.

[65] J. Farjas, P. Roura, Modification of the Kolmogorov-Johnson-Mehl-Avrami rate equation for non-isothermal experiments and its analytical solution, Acta Mater. 54 (2006) 5573–5579, https://doi.org/10.1016/j.actamat.2006.07.037.

[66] J.S. Blázquez, C.F. Conde, A. Conde, Non-isothermal approach to isokinetic crystallization processes: application to the nanocrystallization of HITPERM alloys,

Acta Mater. 53 (2005) 2305–2311, https://doi.org/10.1016/j.actamat.2005.01.037.
[67] J. Wang, S. Niu, T. Guo, H. Kou, J. Li, The FCC to BCC phase transformation kinetics in an Al0.5CoCrFeNi high entropy alloy, J. Alloys Compd. 710 (2017) 144–150, https://doi.org/10.1016/j.jallcom.2017.03.249.
[68] C.P. Jiang, Z.H. Huang, Grain size effect on mechanical properties of titanium alloy, Key Eng. Mater. 626 (2015) 548–552. https://doi.org/10.4028/www.scientific.net/KEM.626.548.
[69] A.G. Dowson, Precipitation-hardening of metals, Br. Dent. J. 90 (1951) 205–211.
[70] D.G. Lee, S. Lee, Y. Lee, Effect of precipitates on damping capacity and mechanical properties of Ti-6Al-4V alloy, Mater. Sci. Eng. A. 486 (2008) 19–26, https://doi.org/10.1016/j.msea.2007.08.053.
[71] S. Cao, Y. Zou, C. Voon Samuel Lim, X. Wu, Review of laser powder bed fusion (LPBF) fabricated Ti-6Al-4V: process, post-process treatment, microstructure, and property, Light Adv. Manuf. 2 (2021) 1–20, https://doi.org/10.37188/lam.2021.020.
[72] H.C. Kaushik, S.I. Shakil, B.S. Amirkhiz, M. Mohammadi, E. Asadi, M. Haghshenas, A. Hadadzadeh, Indentation strain rate sensitivity of laser-powder bed fused and electron beam melted Ti-6Al-4V, Vac 195 (2022), 110690, https://doi.org/10.1016/j.vacuum.2021.110690.
[73] J. Ma, J. Tian, M. Yan, Z. Chen, J. Shen, J. Wu, Defect analysis and 2D/3D-EBSD investigation of an electron beam melted Ti-6Al-4V alloy, Mater. Char. 166 (2020), 110440, https://doi.org/10.1016/j.matchar.2020.110440.
[74] H. Fan, Y. Liu, S. Yang, Martensite decomposition during post-heat treatments and the aging response of near-α Ti–6Al–2Sn–4Zr–2Mo (Ti-6242) titanium alloy processed by selective laser melting (SLM), Journal of Micromechanics and Molecular Physics 6 (2021), 2050018, https://doi.org/10.1142/S2424913020500186.